Chemical Engineering Journal 108 (2005) 51–58

Chemical Engineering Journal

www.elsevier.com/locate/cej

# Modeling of a compact plate-fin reformer for methanol steam reforming in fuel cell systems

Liwei Pan, Shudong Wang*

*Dalian Institute of Chemical Physics, Chinese Academy of Sciences, Dalian 116023, PR China*

Received 30 September 2004; received in revised form 19 December 2004; accepted 23 December 2004

**Abstract**

The characteristics of a compact plate-fin reformer (PFR) which integrates endothermic and exothermic reactions into one unit have been investigated by experiment as well as by numerical simulation. One reforming chamber was integrated with two vaporization chambers and two combustion chambers to constitute a single unit of PFR. In the PFR, which is based on a plate-fin heat exchanger, catalytic combustion of the reforming gas is used to simulate the fuel cell anode off gas (AOG) which supplies the necessary heat for the methanol steam reforming. Temperature distributions in all chambers and composition distribution in reforming chamber have been studied, and the effect of the ratio of $H_2O/CH_3OH$ on the performance of the PFR has also been investigated. A model of the PFR was derived using a three-dimensional numerical model for a cross-current flow arrangement. Theoretical predictions of the temperature distributions in the PFR were in good agreement with experimental values. In addition, the numerical model was able to accurately predict the methanol conversion and the reformate composition in reforming chamber.


*Keywords:* Plate-fin reformer; Methanol; Steam reforming; Simulation; Fuel cell

## 1. Introduction

Hydrogen is generally expected to play an important role in future energy systems. In recent years, much attention has been paid to the use of hydrogen as an energy carrier in fuel cells and mobile vehicles, due to its high-efficiency and very low to zero pollution [1]. In addition, due to their high-energy storage density, liquid fuels such as primary alcohols, gasoline and diesel are attractive for fuel cell application. The two top fuel contenders for the fuel cell market today are methanol and gasoline. From the technological point of view, methanol clearly has distinct advantages as a fuel for fuel cell vehicle applications: methanol is liquid at atmospheric conditions and has a high hydrogen-to-carbon ratio relative to gasoline, and it can be reformed to hydrogen at much lower temperatures (200–300 °C), and is more efficient as compared to gasoline (700–800 °C). In addition, methanol is an environmentally friendly fuel, as it is readily biodegradable in air, soil and water. When methanol is used in a fuel cell vehicle, emissions are extremely low.

Steam reforming of methanol reaction has been a highly developed and thoroughly studied process [2–8]. It can offer the highest maximum hydrogen content in the product gas (75%) while maintaining a high selectivity towards carbon dioxide. On the other hand, steam reforming is an endothermic reaction which requires heat supply from an external source. This can be met by the combustion of the fuel cell anode off gas (AOG) in a fuel cell system. Currently, increasing attention is being paid to the low temperature steam reforming of methanol to produce hydrogen as the fuel in fuel cells [9–13].

For the last 10 years, rapidly growing interest in fuel cells and hydrogen technologies has aroused continuing efforts to

*Abbreviations:* AOG, fuel cell anode off gas; HEX, heat-exchanger; PFR, plate-fin reformer; PROX, CO preferential oxidation; RWGS, reverse WGS reaction; SR, steam reforming reaction

* Corresponding author. Tel.: +86 411 8466 2365; fax: +86 411 8466 2365.
*E-mail address:* wangsd@dicp.ac.cn (S. Wang).

1385-8947/$ – see front matter © 2005 Elsevier B.V. All rights reserved.
doi:10.1016/j.cej.2004.12.042

**Nomenclature**

| | |
|---|---|
| $A$ | pre-exponential factor |
| $C$ | concentration (mol/m$^3$) |
| $E$ | internal energy |
| $g$ | gravitational force |
| $h$ | sensible enthalpy, $\int_{T_{\text{ref}}}^{T} c_p \, \mathrm{d}T$ |
| $\Delta H$ | heat energy of reaction (J/mol) |
| $k_{\text{eff}}$ | effective thermal conductivity (W m$^{-1}$ K$^{-1}$) |
| $m_i$ | the mass fraction of species $i$ |
| $M_i$ | molecular weight (kg/mol) |
| $P$ | pressure (Pa) |
| $R$ | universal gas constant |
| $S_{\text{h}}$ | volumetric heat source |
| $T$ | Temperature (K) |
| $u$ | velocity (m/s) |

*Greek letters*

| | |
|---|---|
| $\mu$ | viscosity (Pa S) |
| $\rho$ | density (kg/m$^3$) |
| $\tau$ | stress tensor |

*Subscripts*

| | |
|---|---|
| $k$ | chamber (1: combustion chamber, 2: reforming chamber) |
| op | operating condition |
| out | outlet |
| 0 | inlet |

develop small-scale fuel processors and hydrogen production systems. The trend is to develop more compact and simpler reformers. Starting from the conventional "long tube" refinery-type steam reformer, fuel cell developers shifted towards the more compact "heat exchange"-type steam reformers. Plate-type reformers are now undergoing development and testing for fuel cell applications [14–18]. The main concept of the plate-type reformers is coupling endothermic reforming reaction with exothermic reaction. Hunter and McGuire were among the first ones in suggesting the coupling of endothermic with exothermic reaction by means of indirect heat transfer [19]. They considered catalytic heat exchangers in which catalytic combustion or a highly exothermic reaction is used as the heat source for an endothermic reaction. The feasibility of combining in an autothermal micro-channel reactor for methanol reforming with total oxidation of methanol as the heat source has been demonstrated by Reuse et al. [20]. The coupling of methane steam reforming with catalytic combustion in adjacent channels has also been studied by Zanfir and Gavriilidis [18] and Frauhammer et al. [21].

In the present work, a highly favorable design for efficient coupling of an endothermic steam reforming reaction with a heat source has been proposed, and the main feature is the adopting of a compact plate-fin reformer (PFR) derived from a plate-fin heat exchanger. The plate-fin configuration offers a high degree of compactness and minimizes heat transfer resistance. In this paper, we have studied a reaction system, in which part of reforming gas catalytic combustion coupled with methanol steam reforming. In addition, a three-dimensional numerical model was derived for cross-current flow arrangement.

## 2. Plate-fin reformer

One reforming chamber, two vaporization chambers and two combustion chambers were integrated into a unit of compact plate-fin reformer (PFR). The scheme of this concept is given in Fig. 1. For a more detailed examination of the thermal behavior of the reformer, it is useful to investigate the temperature distributions of the various chambers of the PFR. Fifteen thermocouples, placed in the PFR as defined in Fig. 1, were employed. Each thermocouple could be moved along the axial direction of the chambers so that it could measure any temperature point along the axial positions. Each chamber of the reformer had a plate-fin configuration, and a cross-flow mode was arranged in alternate chambers (Fig. 2). In order to increase the rate of heat transfer, perforated fin was adopted in our research. The specification of the fin is also shown in Fig. 2.

The PFR, which had a volume of 150 mm × 125 mm × 40 mm, was made of stainless steel. First, 45.19 g of the combustion pellet catalyst of Pt/$Al_2O_3$ (catalyst were designed in our lab) and 158.40 g of the reforming pellet catalyst of Cu/ZnO/$Al_2O_3$ (catalyst CB-7 from the Catalyst Plant of Sichuan Chemical Works Group Ltd.) were loaded into the PFR. The catalyst of Cu/ZnO/$Al_2O_3$ was ground and sieved, then the catalyst sample with appropriate particle diameter was obtained for loading into the reforming chamber compactly. A particle size of 0.442–0.681 mm was used in this work. If air and hydrogen are mixed directly at the entrance of the combustion chamber, the temperature will increased so quickly that it will lead to an uncontrolled run-away of the

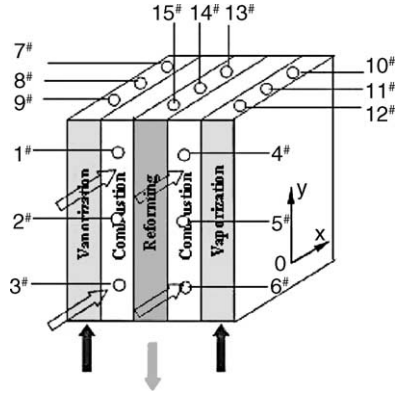


Fig. 1. Configuration of the PFR, in which catalytic combustion is coupled with methanol steam reforming in a cross-flow mode. The locations of the thermocouples in the PFR are also shown.

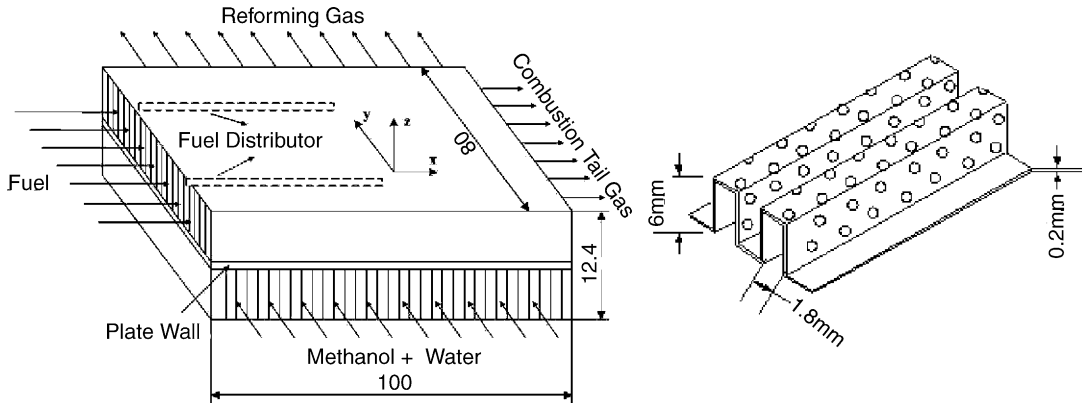


Fig. 2. Typical cross-flow arrangement of PFR (a) cross-flow arrangement and the computational domain used to model the PFR (b) configuration of perforated fin.

exothermic reaction. Therefore, two $H_2$ distributors, which functioned to make the hydrogen-rich gas to distribute uniformly, were arranged inside the combustion chamber so that excessive temperature excursions can be avoided (Fig. 2).

## 3. Experimental procedure

The $Cu/ZnO/Al_2O_3$ catalyst was initially in a calcined oxidation state, and should be activated in a reducing atmosphere. Temperature programmed reduction of the steam reforming catalyst was performed at atmospheric pressure in the reforming chamber of the PFR. The steam reforming catalyst was heated in a reducing gas stream at a linearly programmed rate of 4 °C/min from 25 to 300 °C. The reduction was performed in a $H_2$–$N_2$ mixture (3 mol% $H_2$) flowing at a rate of 500 mL STP/min. The reduction was maintained at 300 °C until the concentration of $H_2$ became unchanged after the reducing gas passed through the reforming chamber.

A scheme of the hydrogen generation system is depicted in Fig. 3. During the start-up, hydrogen and air from gas cylinders were introduced into the combustion chambers to heat up the reforming chamber. When the reforming chamber reached the desired temperature, distilled water and methanol were first pre-mixed and then fed into the two vaporization chambers through a pulseless pump. After being gasified, the reactants were fed into the reforming chamber. After the reforming reaction was progressing steadily, a part of the reforming gas produced in the reforming chamber was sent to the combustion chambers, while hydrogen from the cylinder, which was used for the start-up, was shut off. In practical applications, if the PFR is used to supply hydrogen for a fuel cell, the anode off gases from the fuel cell will be fed into the combustion chambers. In our experiment, the product gas from the reforming chamber was cooled to remove

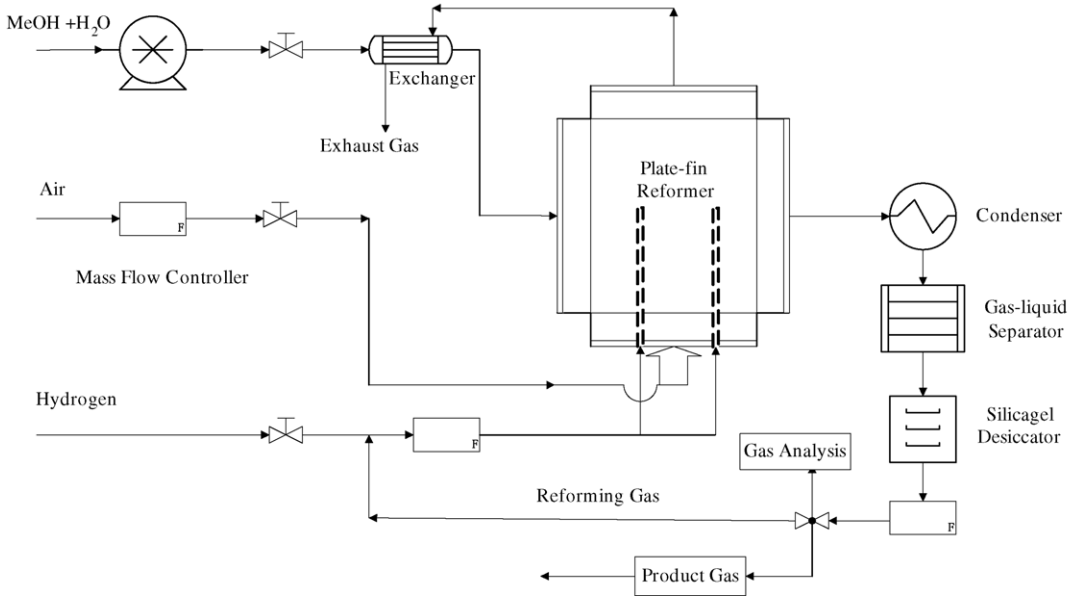


Fig. 3. Scheme of the plate-fin reformer experimental set-up.

of unreacted methanol and moisture, and then was analyzed with an on-line gas chromatograph (GC-14C, Shimadzu Co.), using a thermal conductivity detector (TCD), and with argon as the carrier gas. The total flow rate of the dry product stream was measured by a mass flow meter.

## 4. Numerical model

A comprehensive three-dimensional model has been developed for a PFR in order to determine the composition and temperature distributions inside the reformer. The computational domain for the PFR is shown in Fig. 2(a). Thus, three different domains could be identified: chamber 1, where catalytic combustion of hydrogen and air takes place, chamber 2, where the methanol steam reforming occurs and the plate wall. The numerical simulation of the PFR was performed with three-dimensional, steady state in a cross-flow arrangement and Standard $k$–$\varepsilon$ Model flow system. The numerical model simulates the catalytic combustion of the reforming gas coupling the methanol steam reforming. The governing equations for the modeling are written as follows:

Continuity equation

$$\frac{\partial}{\partial x_i}(\rho_k u_{ki}) = 0 \tag{1}$$

Momentum equation

$$\frac{\partial}{\partial x_j}(\rho_k u_{ki} u_{kj}) = -\frac{\partial p_k}{\partial x_i} + \frac{\partial \tau_{ij}}{\partial x_j} + \rho_k g_i + S_{ki} \tag{2}$$

where

$$\tau_{ij} = \left[\mu_k \left(\frac{\partial u_{ki}}{\partial x_j} + \frac{\partial u_{kj}}{\partial x_i}\right)\right] - \frac{2}{3}\mu_k \frac{\partial u_{kl}}{\partial x_l}\delta_{ij} \tag{3}$$

$$S_{ki} = -\left(\sum_{j=1}^{3} D_{ij}\mu_k u_{kj} + \sum_{j=1}^{3} C_{ij}\frac{1}{2}\rho(u_{kj}|u_{kj}|)\right) \tag{4}$$

In the momentum equation (2), the pellet catalysts were modeled as a porous media by the addition of a momentum source term to the standard fluid flow equations. The porous media model can be used for solving problems concerning flows through packed beds and perforated plates. $S_i$ is the source term for the $i$-direction ($x$, $y$, or $z$) momentum equation, and $D$ and $C$ are prescribed matrices.

Energy equation

$$\frac{\partial}{\partial x_i}(u_{ki}(\rho_k E_k + p_k)) = \frac{\partial}{\partial x_i}\left((k_{\text{eff}})_k \frac{\partial T_k}{\partial x_i} - \sum_{j'} h_{kj'} J_{kj'} + u_{kj}(\tau_{ij})_{\text{eff},k}\right) + \Delta H_{\text{h}} + (1-\gamma)S_{\text{s}}^{\text{h}} \tag{5}$$

The effective thermal conductivity in the porous medium, $k_{\text{eff}}$, is computed as the volume average of the fluid conductivity and the solid conductivity:

$$k_{\text{eff}} = \gamma k_{\text{f}} + (1-\gamma)k_{\text{s}} \tag{6}$$

In Eqs. (5) and (6), $S_{\text{s}}^{\text{h}}$ is the solid medium enthalpy source term, $k_{\text{f}}$ is the fluid phase thermal conductivity, $k_{\text{s}}$ is the solid medium thermal conductivity, $\gamma$ is the porosity of the medium.

Energy equation in the plate wall regions

$$\frac{\partial}{\partial t}(\rho h) + \frac{\partial}{\partial x_i}(\rho u_i h) = \frac{\partial}{\partial x_i}\left(k\frac{\partial T}{\partial x_i}\right) + S_{\text{h}} \tag{7}$$

Equation of state for ideal gas

$$\rho_k = \frac{(p_{\text{op}})_k}{RT_k \sum_{i'} m'_{ki}/M'_{ki}} \tag{8}$$

The catalytic combustion of $H_2$ can be represented by the following one-step reaction (9). The reaction rate of $H_2$ over the Pt catalyst was calculated with Eq. (10) proposed by Mitani and Williams [22]

$$H_2 + \tfrac{1}{2}O_2 = H_2O \tag{9}$$

$$R = AC_{H_2}C_{O_2}\exp\left(\frac{-E}{RT}\right) \tag{10}$$

with $A = 2.196 \times 10^{12}\ \text{mol}^{-1}\ \text{cm}^3\ \text{s}^{-1}$, $E = 109.2\ \text{kJ mol}^{-1}$.

Purnama et al. [23] have illustrated the reaction schemes for methanol steam reforming over a $Cu/ZnO/Al_2O_3$ catalyst as follows: (i) the methanol steam reforming (SR) reaction (Eq. (11)) and (ii) the reverse water gas shift (rWGS) reaction (Eq. (12)). They also indicated that CO is a consecutive product by the rWGS reaction. The same results were obtained by Agrell et al. [24]. The power rate law and the kinetic reaction parameters of the SR reaction and the reverse WGS reaction were given below [23]:

$$CH_3OH + H_2O \xrightarrow{k_1} CO_2 + 3H_2 \tag{11}$$

$$CO_2 + H_2 \underset{k_{-2}}{\overset{k_2}{\rightleftharpoons}} CO + H_2O \tag{12}$$

$$r_{\text{SR}} = k_1 P_{CH_3OH}^m P_{H_2O}^n, \quad m = 0.6,\ n = 0.4$$

apparent $E_{\text{a}} = 76\ \text{kJ mol}^{-1}$, $k_0 = 8.8 \times 10^8\ \text{s}^{-1}\ \text{g}_{\text{cat}}^{-1}$

$$r_{\text{rWGS}} = k_2 P_{CO_2} P_{H_2} - k_{-2} P_{H_2O} P_{CO}$$

apparent $E_{\text{a}} = 108\ \text{kJ mol}^{-1}$, $k_0 = 6.5 \times 10^9\ \text{bar}^{-1}\ \text{s}^{-1}\ \text{g}_{\text{cat}}^{-1}$.

FLUENT software was used to solve the mathematical model. The distributions of stream-wise velocity and temperature were assumed to be uniform at the inlet boundary of both the combustion chamber and the reforming chamber, except for the distribution of hydrogen. The velocity components in the $z$-direction at the inlet boundary were assumed to be zero. At the outlet of the computational domain, the flow and thermal fields were treated to obey the zero diffusion flux for all flow variables in the axial direction.

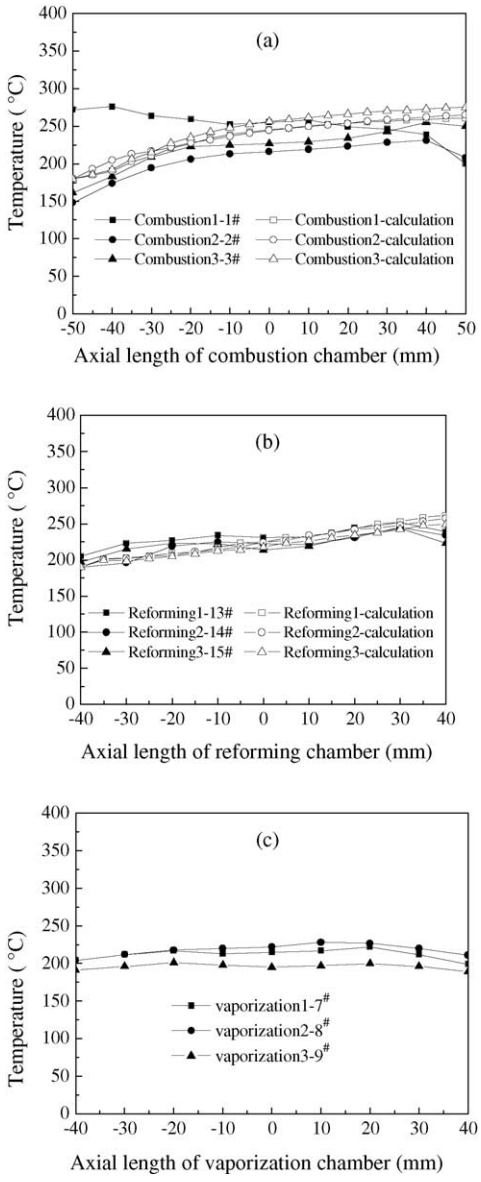


Fig. 4. Axial temperature distribution in the whole PFR ($H_2O/CH_3OH = 1.2$; flux of $CH_3OH$–$H_2O$ was 5 mL/min; 7.7 L/min air and 2.9 L/min reforming gas were fed into the combustion chambers).

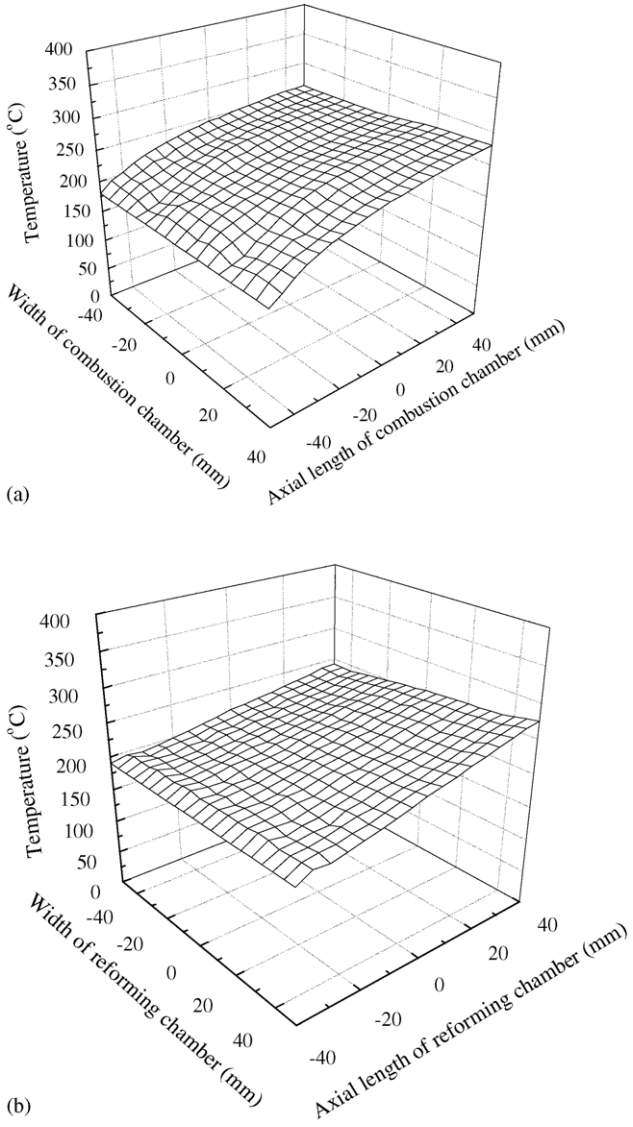


Fig. 5. Calculated temperature distributions in different chambers of PFR ($H_2O/CH_3OH = 1.2$; flux of $CH_3OH$–$H_2O$ was 5 mL/min; 7.7 L/min air and 2.9 L/min reforming gas were fed into the combustion chambers).

## 5. Results and discussion

For a more detailed examination of the thermal behavior of the reformer, it is useful to investigate the distributions in different chambers of the PFR. Fifteen thermocouples, placed in the PFR as defined in Fig. 1, were used to detect the temperature distributions in the whole PFR, and the results are shown in Fig. 4. The axial temperatures of the reforming chamber and the vaporization chambers were uniform, while those in the combustion chambers were also uniform, except for the points at the entrance and the exit of the combustion chamber. At the entrances of the combustion chambers, the combustion gas was distributed unevenly, thus resulting in obvious temperature differences. At the exit of the combustion chambers, a design for heat recovery caused a decrease in temperatures.

In order to establish a reference point for the calculations, the following conditions were employed: 5 mL/min $H_2O$–$CH_3OH$ (molar ratio = 1.2:1) were fed into the reforming chamber, while 7.7 L/min air and 2.9 L/min reforming gas were fed into the combustion chambers.

Fig. 5 shows the calculation results of the temperature distributions in one combustion chamber and one reforming chamber. To validate the calculation results in detail, they were compared with the experiment. Fig. 4(a) and (b) shows the comparison between the calculation and experiment about temperatures at same locations in the combustion chamber and reforming chamber. The overall trends in temperature variation with the axial length of the chamber agreed quite well. The calculation shows a little difference in the catalytic

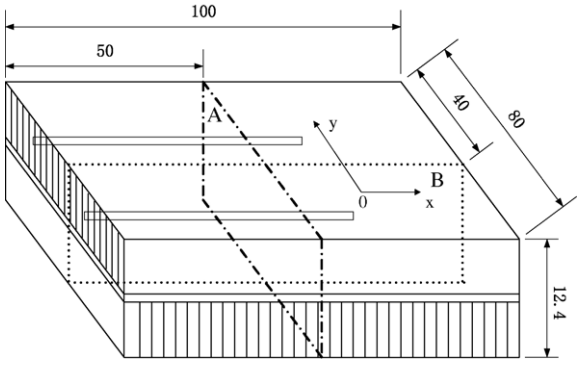


Fig. 6. Locations of planes A and B defined in PFR.

combustion performance with those of the experiment. This was probably caused by the fact that the performance of the $H_2$ distributor did not turn out as what was designed. More hydrogen-rich gas was distributed at the place near $1^{\#}$ by the actual $H_2$ distributor, which made the temperature of combustion $1–1^{\#}$ be a little higher than others in experimental results.

For a more detailed examination of the thermal behavior of the reactor, it is meaningful to present the cross-sectional temperature distributions in planes A and B, as shown in Fig. 6. The calculated results of these cross-sectional temperature distributions were also presented in Fig. 7, and it shows 10–40 °C temperature difference is needed to transfer heat across the plate wall.

The proton exchange membrane fuel cell (PEMFC), which is easily deactivated when carbon monoxide is present, requires the CO to be below 50 ppm. Thus, it is necessary that the model should be able to accurately predict the composition of CO in the reforming gas. In this work, both CO and

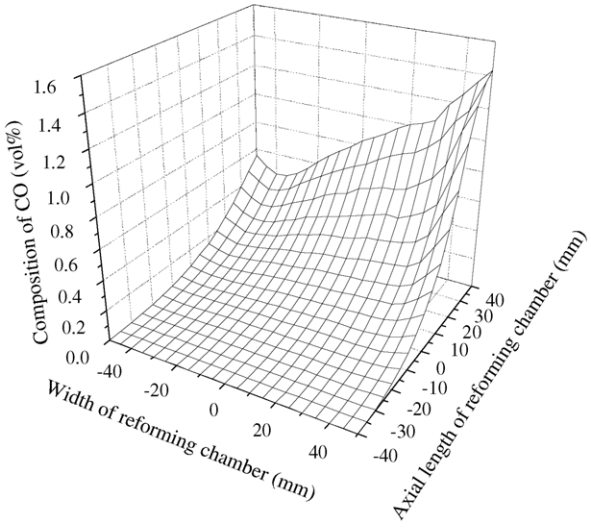


Fig. 8. Calculated composition distributions of CO in reforming chamber ($H_2O/CH_3OH$ = 1.2; flux of $CH_3OH–H_2O$ was 5 mL/min; 7.7 L/min air and 2.9 L/min reforming gas were fed into the combustion chambers).

$H_2$ composition distributions in the reforming gas, which include water–vapor, were calculated (Figs. 8 and 9.) The trend of the composition distribution of CO in reforming chamber was in agreement with the temperature distributions showed in Fig. 5(b).

The influence of the molar ratio of $H_2O/CH_3OH$ on the composition of the reforming gas (dry product stream) was investigated by the experiment and numerical calculation, and the conditions used for comparing between the experiment and calculation are given in Table 1. In Fig. 10, the content of $H_2$ is kept at about 74.5% with different molar ratios of $H_2O/CH_3OH$. The content of CO decreases with

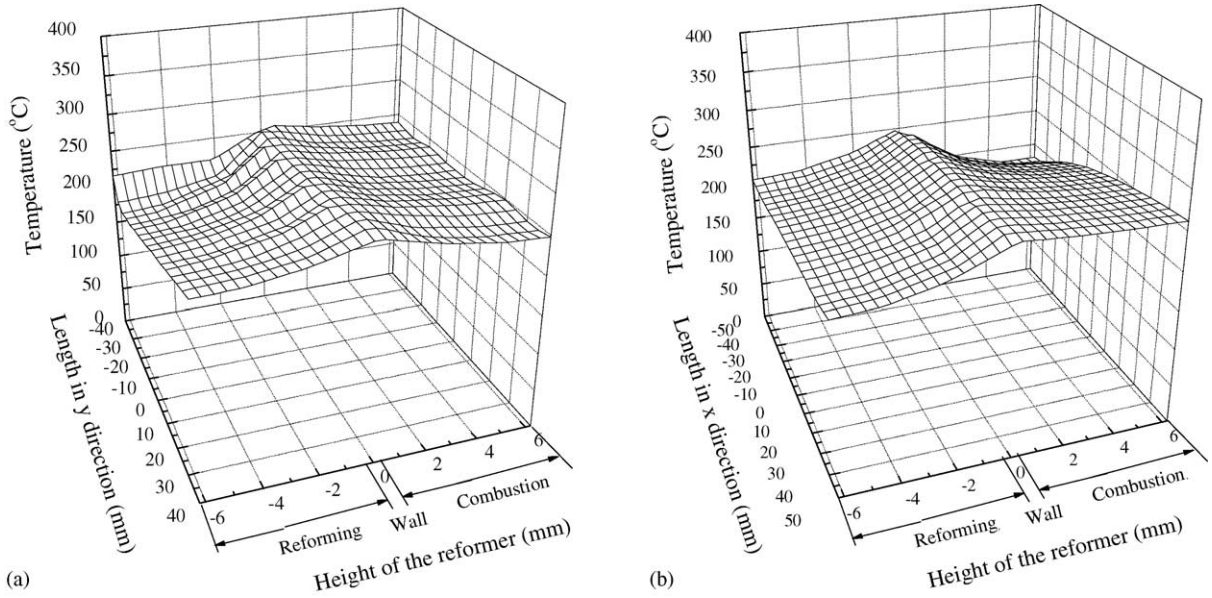


Fig. 7. Calculated temperature distributions in planes A and B ($H_2O/CH_3OH$ = 1.2; flux of $CH_3OH–H_2O$ was 5 mL/min; 7.7 L/min air and 2.9 L/min reforming gas were fed into the combustion chambers).

Table 1
Conditions used for comparing between the experiment and calculation

| Chamber 1 (catalytic combustion) | | Chamber 2 (methanol steam reforming) | |
|---|---|---|---|
| Air inlet (L/min) | Reforming gas inlet (L/min) | Molar ratio of $H_2O/CH_3OH$ | Flow rate (mL/min) |
| 7.7 | 2.9 | 1.2 | 5 |
| 7.7 | 2.8 | 1.3 | 5 |
| 7.7 | 2.9 | 1.4 | 5 |
| 8.0 | 2.9 | 1.5 | 5 |
| 8.0 | 3.0 | 1.6 | 5 |

the increasing of the $H_2O/CH_3OH$ ratio, while it can be controlled to be less than 1%. The calculation results show a higher CO composition than that of the experiment under higher molar ratio of the $H_2O/CH_3OH$. This may due to the fact that the calculated reforming temperature is a little higher than the actual value.

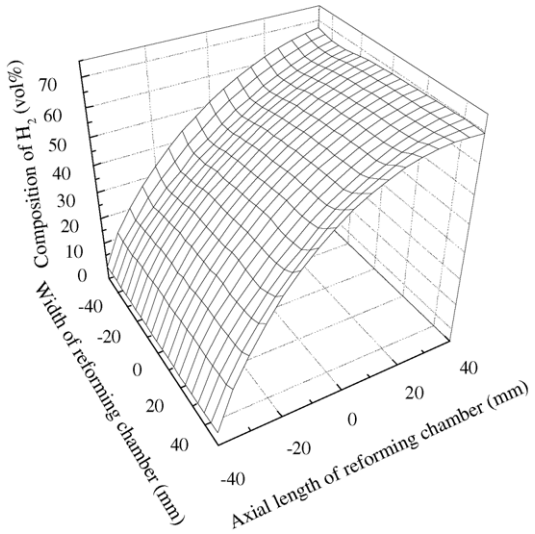


Fig. 9. Calculated composition distributions of $H_2$ in reforming chamber ($H_2O/CH_3OH = 1.2$; flux of $CH_3OH$–$H_2O$ was 5 mL/min; 7.7 L/min air and 2.9 L/min reforming gas were fed into the combustion chambers).

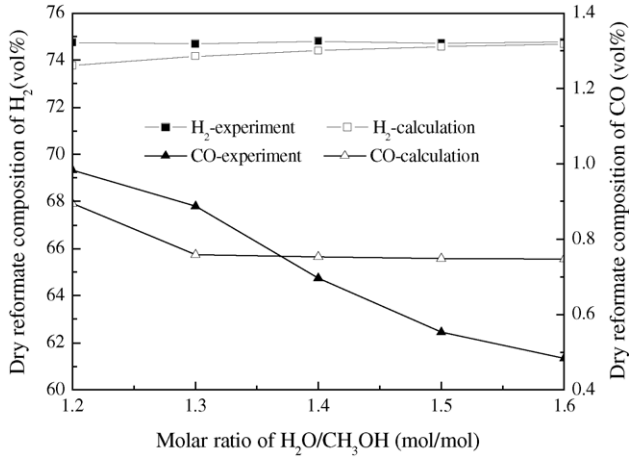


Fig. 10. Influence of the molar ratio of $H_2O/CH_3OH$ on composition of reforming gas.

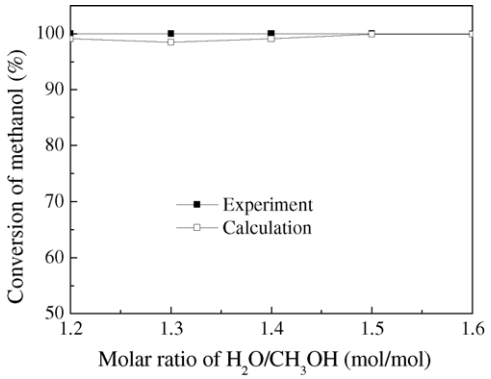


Fig. 11. Comparison between computation and experiment for the methanol conversion as a function of the molar ratio of $H_2O/CH_3OH$.

To understand the characteristics of the methanol steam reforming in the PFR, the conversion of the methanol as a function of the molar ratio of $H_2O/CH_3OH$ is shown in Fig. 11. The conversion of methanol steam reforming was calculated by the following equation:

$$\text{conversion of methanol}\,(\%) = \frac{C_0 - C_{\text{out}}}{C_0} \times 100 \qquad (13)$$

where $C_0$ and $C_{\text{out}}$ are the inlet and outlet molar concentration, respectively.

From a comparison between the calculated and experimental results, it can be found that the conversion of methanol in steam reforming could reach up to approximately 100% under different molar ratio of $H_2O/CH_3OH$, with an appropriate flux of reactant.

## 6. Conclusions

The characteristics of a compact plate-fin reformer (PFR) which integrates endothermic and exothermic reactions into one unit have been investigated by experiment as well as by numerical simulation. The reformer can integrate methanol steam reforming, vaporization, catalytic combustion and heat recovery into one unit. In the experiment, catalytic combustion of part of the reforming gas was adopted to simulate the combustion of fuel cell anode off gas (AOG), and was coupled with methanol steam reforming in a cross-flow mode. The isothermality of the system is the key issue during the performance of the PFR. Both the experimental and numerical

simulation results showed that temperature distributions were uniform in different chambers of the PFR. Besides, both internal plate-fins and external catalytic combustion were used to enhance heat transfer of the reformer, which allowed the requirement of only small temperature difference for heat transfer across the plate wall. The calculated results also could accurately predict the conversion of methanol and the reformate composition.

## Acknowledgements

The authors acknowledge the support of the Special Fund for Major State Basic Research Projects (G2000026401) of the Ministry of Science and Technology of China. We also gratefully acknowledge the help of Associate Professor Shiying Li in reformer design, and Associate Professor Zhongshan Yuan for the supplying of the combustion catalysts. Also, the assistance of Mr. Nan Liu in the experiments and the helpful discussions of Dr. Sheng Wang in the FLUENT software were greatly appreciated.

## References

[1] J.C. Amphlett, R.F. Mann, R.D. Weir, Hydrogen production by the catalytic steam reforming of methanol. Part 3. Kinetics of methanol decomposition using C18HC catalyst, Can. J. Chem. Eng. 66 (6) (1988) 950–956.

[2] K. Takahashi, N. Takezawa, H. Kobayashi, The mechanism of steam reforming of methanol over a copper-silica catalyst, Appl. Catal. A: Gen. 2 (6) (1982) 363–366.

[3] C.J. Jiang, D.L. Trimm, M.S. Wainwright, N.W. Cant, Kinetic mechanism for the reaction between methanol and water over a Cu–ZnO–$Al_2O_3$ catalyst, Appl. Catal. A: Gen. 97 (2) (1993) 145–158.

[4] N. Iwasa, S. Kudo, H. Takahashi, S. Masuda, N. Takezawa, Highly selective supported Pd catalysts for steam reforming of methanol, Catal. Lett. 19 (1993) 211.

[5] J.C. Amphlett, K.A.M. Creber, J.M. Davis, R.F. Mann, B.A. Peppley, D.M. Stokes, Hydrogen production by steam reforming of methanol for polymer electrolyte fuel cells, Int. J. Hydrogen Energy 19 (2) (1994) 131–137.

[6] K. Miyao, H. Onodera, N. Takezawa, Highly active copper catalysts for steam reforming of methanol. Catalysts derived from Cu/Zn/Al alloys, React. Kinet. Catal. Lett. 53 (2) (1994) 379–383.

[7] N. Iwasa, S. Masuda, N. Ogawa, N. Takezawa, Steam reforming of methanol over Pd/ZnO: effect of the formation of PdZn alloys upon the reaction, Appl. Catal. A: Gen. 125 (1) (1995) 145–157.

[8] J.P. Breen, F.C. Meunier, J.R.H. Ross, Mechanistic aspects of the steam reforming of methanol over a CuO/ZnO/$ZrO_2$/$Al_2O_3$ catalyst, Chem. Commun. 22 (1999) 2247–2248.

[9] J. Bravo, A. Karim, T. Conant, G.P. Lopez, A. Datye, Wall coating of a CuO/ZnO/$Al_2O_3$ methanol steam reforming catalyst for microchannel reformers, Chem. Eng. J. 101 (1–3) (2004) 113–121.

[10] G.-G. Park, D.J. Seo, S.-H. Park, Y.-G. Yoon, Ch.-S. Kim, W.-L. Yoon, Development of microchannel methanol steam reformer, Chem. Eng. J. 101 (1–3) (2004) 87–92.

[11] C. Horny, L. Kiwi-Minsker, A. Renken, Micro-structured string-reactor for autothermal production of hydrogen, Chem. Eng. J. 101 (1–3) (2004) 3–9.

[12] C. Fukuhara, H. Ohkura, Y. Kamata, Y. Murakami, A. Igarashi, Catalytic properties of plate-type copper-based catalysts, for steam reforming of methanol, on an aluminum plate prepared by electroless plating, Appl. Catal. A: Gen. 273 (1/2) (2004) 125–132.

[13] J.K. Lee, J.B. Ko, D.H. Kim, Methanol steam reforming over Cu/ZnO/$Al_2O_3$ catalyst: kinetics and effectiveness factor, Appl. Catal. A: Gen. 278 (1) (2004) 25–35.

[14] A.M. De Groote, G.F. Froment, Th. Kobylinski, Synthesis gas production from natural gas in a fixed bed reactor with reversed flow, Can. J. Chem. Eng. 74 (1996) 735–742.

[15] L. Ma, D.L. Trimm, Alternative catalyst bed configurations for the autothermic conversion of methane to hydrogen, Appl. Catal. A: Gen. 138 (1996) 265–273.

[16] D. Wolf, M. Höhenberger, M. Baerns, External mass and heat transfer limitations of the partial oxidation of methane over a Pt/MgO catalyst—consequences for adiabatic reactor operation, Ind. Eng. Chem. Res. 36 (1997) 3345–3353.

[17] A.K. Avic, D.L. Trimm, Z. İlsen Önsan, Heterogeneous reactor modeling for simulation of catalytic oxidation and steam reforming of methane, Chem. Eng. Sci. 56 (2001) 641–649.

[18] M. Zanfir, A. Gavriilidis, Catalytic combustion assisted methane steam reforming in a catalytic plate reactor, Chem. Eng. Sci. 58 (2003) 3947–3960.

[19] J.B. Hunter, G. McGuire, Method and apparatus for catalytic heat exchange, US Patent 4,214,867 (1980).

[20] P. Reuse, A. Renken, K. Haas-Santo, O. Görke, K. Schubert, Hydrogen production for fuel cell application in an autothermal micro-channel reactor, Chem. Eng. J. 101 (1–3) (2004) 133–141.

[21] J. Frauhammer, G. Eigenberger, L.V. Hippel, D. Arntz, A new reactor concept for endothermic high-temperature reactions, Chem. Eng. Sci. 54 (1999) 3661–3670.

[22] T. Mitani, F.A. Williams, Studies of cellular flames in hydrogen–oxygen–nitrogen mixture, Combust. Flame 39 (1980) 169–190.

[23] H. Purnama, T. Ressler, R.E. Jentoft, H. Soerijanto, R. Schlögl, R. Schomäcker, CO formation/selectivity for steam reforming of methanol with a commercial CuO/ZnO/$Al_2O_3$ catalyst, Appl. Catal. A: Gen. 259 (1) (2004) 83–94.

[24] J. Agrell, H. Birgersson, M. Boutonnet, Steam reforming of methanol over Cu–ZnO–$Al_2O_3$ catalyst: a kinetic analysis and strategies for suppression of CO formation, J. Power Sour. 106 (12) (2002) 249–257.